International Journal of Radiation Oncology biology • physics

www.redjournal.org

Biology Contribution

Assessing Cardiac Injury in Mice With Dual Energy-MicroCT, 4D-MicroCT, and MicroSPECT Imaging After Partial Heart Irradiation

Chang-Lung Lee, PhD,* Hooney Min, BS,* Nicholas Befera, MD,† Darin Clark, BS,† Yi Qi, MD,† Shiva Das, PhD,* G. Allan Johnson, PhD,† Cristian T. Badea, PhD,† and David G. Kirsch, MD, PhD*,‡

**Department of Radiation Oncology; †Center for In Vivo Microscopy, Department of Radiology; and ‡Department of Pharmacology and Cancer Biology, Duke University Medical Center, Durham, North Carolina*

Received Aug 7, 2013, and in revised form Oct 28, 2013. Accepted for publication Nov 20, 2013

Summary

We used a micro-irradiator to deliver tangent field x-rays to the left chest wall of mice to develop a mouse model of cardiac injury after partial heart irradiation. We noninvasively assessed myocardial vascular permeability and cardiac function using dual energy (DE) and 4-dimensional (4D)-microCT with nanoparticle-based contrast agents. We showed that in mice, DE-microCT and 4D-microCT can provide novel imaging approaches to investigate cardiac pathophysiology after partial heart irradiation, which is complementary to myocardial perfusion obtained with microSPECT.

Purpose: To develop a mouse model of cardiac injury after partial heart irradiation (PHI) and to test whether dual energy (DE)-microCT and 4-dimensional (4D)-microCT can be used to assess cardiac injury after PHI to complement myocardial perfusion imaging using micro-single photon emission computed tomography (SPECT).

Methods and Materials: To study cardiac injury from tangent field irradiation in mice, we used a small-field biological irradiator to deliver a single dose of 12 Gy x-rays to approximately one-third of the left ventricle (LV) of Tie2Cre; $p53^{FL/+}$ and Tie2Cre; $p53^{FL/-}$ mice, where 1 or both alleles of p53 are deleted in endothelial cells. Four and 8 weeks after irradiation, mice were injected with gold and iodinated nanoparticle-based contrast agents, and imaged with DE-microCT and 4D-microCT to evaluate myocardial vascular permeability and cardiac function, respectively. Additionally, the same mice were imaged with microSPECT to assess myocardial perfusion.

Results: After PHI with tangent fields, DE-microCT scans showed a time-dependent increase in accumulation of gold nanoparticles (AuNp) in the myocardium of Tie2Cre; $p53^{FL/-}$ mice. In Tie2Cre; $p53^{FL/-}$ mice, extravasation of AuNp was observed within the irradiated LV, whereas in the myocardium of Tie2Cre; $p53^{FL/+}$ mice, AuNp were restricted to blood vessels. In addition, data from DE-microCT and microSPECT showed a linear correlation ($R^2 = 0.97$) between the fraction of the LV that accumulated AuNp and the fraction of LV with a perfusion defect. Furthermore, 4D-microCT scans demonstrated that PHI caused a markedly decreased ejection fraction, and higher end-diastolic and end-systolic volumes, to develop in Tie2Cre; $p53^{FL/-}$ mice, which were associated with compensatory cardiac hypertrophy of the heart that was not irradiated.

Conclusions: Our results show that DE-microCT and 4D-microCT with nanoparticle-based contrast agents are novel imaging approaches complementary to microSPECT for noninvasive assessment of the change in myocardial vascular permeability and cardiac function of mice in whom myocardial injury develops after PHI.

Reprint requests to: David G. Kirsch, MD, PhD, Duke University Medical Center, Box 91006, Durham, NC 27708. Tel: (919) 681-8605; E-mail: david.kirsch@duke.edu

C. T. Badea and D. G. Kirsch contributed equally to this study.

Conflict of interest: none.

Supplementary material for this article can be found at www.redjournal.org.

Int J Radiation Oncol Biol Phys, Vol. 88, No. 3, pp. 686–693, 2014
0360-3016/$ - see front matter

Introduction

Radiation therapy (RT) in the postlumpectomy or postmastectomy setting for breast cancer patients has been shown to improve rates of local control and, for some subgroups of patients, rates of survival (1, 2). However, RT to the chest wall can expose the heart to incidental radiation, which can lead to radiation-related heart disease (RRHD) and death (1, 3-6). The overall dose of radiation to the heart and the proportion of the heart irradiated have been reported to correlate with the risk of RRHD (6, 7).

It remains challenging to identify the subset of patients who will experience RRHD and to establish reproducible markers to diagnose RRHD. To develop an early surrogate for RRHD, several clinical trials have used single photon emission computed tomography (SPECT) imaging to assess changes in myocardial perfusion after RT (8, 9). A prospective study (9) used SPECT to examine myocardial perfusion in patients with left-sided breast cancer before and after RT, and showed that radiation causes volume-dependent defects in cardiac perfusion, which can persist even 3 to 6 years after RT (10). Thus, these findings suggest that noninvasive imaging modalities that detect early changes in the irradiated heart may help to identify patients at risk for the development of RRHD at an early stage of pathogenesis.

One underlying mechanism of RRHD is damage to vascular endothelial cells (11-17), which contributes to both microvascular and macrovascular injuries (18). Recently, we demonstrated that the tumor suppressor p53 protects cardiac endothelial cells against radiation (16). After a single dose of 12 Gy or 10 fractions of 3 Gy whole heart irradiation, Tie2Cre; $p53^{FL/-}$ mice, where both alleles of p53 are deleted in endothelial cells, are sensitive to radiation-induced myocardial injury compared with Tie2Cre; $p53^{FL/+}$ littermates, which retain 1 allele of p53 in endothelial cells. Histologic and physiologic examinations indicate that damage to the microvasculature of the heart after irradiation precedes pathologic changes in the myocardium. Thus, imaging biomarkers that assess alterations in vascular permeability are promising surrogates to the noninvasive identification of regions of the myocardium at risk for radiation-induced injury in vivo.

Recently, we demonstrated that dual energy (DE)-microCT is an effective tool for noninvasive assessment of vascular changes in primary tumors after a single therapeutic dose of RT (19). To develop microCT imaging methods to study cardiac injury from tangent field irradiation in mice, we used a small-field biological irradiator to deliver a single dose of 12 Gy x-rays to approximately one-third of the LV of Tie2Cre; $p53^{FL/-}$ and Tie2Cre; $p53^{FL/+}$ mice. To achieve noninvasive and sensitive measurements at both anatomic and functional levels for the murine heart, we performed DE-microCT and 4-dimensional (4D)-microCT with 2 nanoparticle-based contrast agents: a blood-pool liposomal iodine (Lip-I) (20) and a PEGylated gold nanoparticle (AuNp). Theses contrast agents were chosen on the basis of their physical properties and because of their potential for translation into the clinic (21).

Although DE-CT and cardiac 4D-CT are both gaining momentum in the clinic, they are still novel in the preclinical domain to study cardiac injury after RT. Here, we show that DE-microCT and 4D-microCT are effective preclinical imaging approaches that provide not only anatomic but also functional information to enable noninvasive measurement of radiation-induced cardiac injury in mice. For comparison and validation we also assessed cardiac perfusion in the same cohort of mice by microSPECT.

Methods and Materials

Mouse strains

All animal procedures were approved by the Institutional Animal Care and Use Committee at Duke University. Tie2Cre; $p53^{FL/-}$ mice and Tie2Cre; $p53^{FL/+}$ littermates (8 to 10 weeks old), which have been characterized previously (16, 17), were used for experiments.

Radiation

Partial heart irradiation was performed with a small-field biological irradiator, the X-RAD 225 Cx (Precision X-ray). The isocenter was placed in the heart (source-to-subject distance: ~30.75 cm) using cone beam CT. Placement of the isocenter was based on the location of the following landmarks: spinal cord, sternum, and heart with use of the axial, coronal, sagittal images. Treatment was delivered with 2 opposing tangent fields by use of gantry angles of 45° and 225° (Fig. 1A). Irradiation was performed with a rectangular collimator to produce a radiation field of 10 mm × 10 mm at the treatment isocenter. We delivered 225-kVp x-rays with an average dose rate of 300 cGy/min at target depth using a current of 13 mA and a 0.3-mm Cu filter. The dose rate was measured with an ion chamber by members of the Radiation Safety Division at Duke University.

Imaging protocol

Both DE-microCT and 4D-microCT acquisitions were performed with a dual source microCT system developed in the Center for In Vivo Microscopy at Duke explicitly for dynamic and spectral applications. Imaging was performed 4 and 8 weeks after irradiation (Fig. 1B). The mice were intravenously injected with 0.004 mL/g AuNp contrast agent (AuroVist, www.nanoprobes.com) only once on day 0. Three days later the mice were injected again with 0.012 mL/g Lip-I. The use of both types of nanoparticles was necessary to measure vascular permeability in the damaged myocardium (via AuNp, which extravasates after a few days and accumulates in the injured tissue) and to image cardiac function with 4D-microCT (via Lip-I, which remains intravascular). DE-microCT was performed immediately after Lip-I injection, followed by a 4D-microCT acquisition. One day later (ie, day 4) the mice were injected with 99mTc-tetrofosmin (300 ± 79 MBq) and imaged with microSPECT. At 8 weeks, the mice received another intravenous injection of Lip-I (0.012 mL/g) and were scanned again with DE- and 4D-microCT. The following day, the mice were injected with ^{99m}Tc-tetrofosmin (300 ± 79 MBq) and imaged by microSPECT. The free-breathing animals were scanned while under anesthesia induced with 1% isoflurane delivered by nose cone.

The estimated cumulative radiation dose associated with imaging for the entire study was 0.26 Gy for DE-microCT, 0.58 Gy for 4D-microCT, and 1.34 Gy for microSPECT.

Dual energy-microCT

Images from DE-microCT were used to determine the fraction of damaged LV, which was estimated by semiautomatic segmentation using the Segment Assistant and VoxelCount plugins for

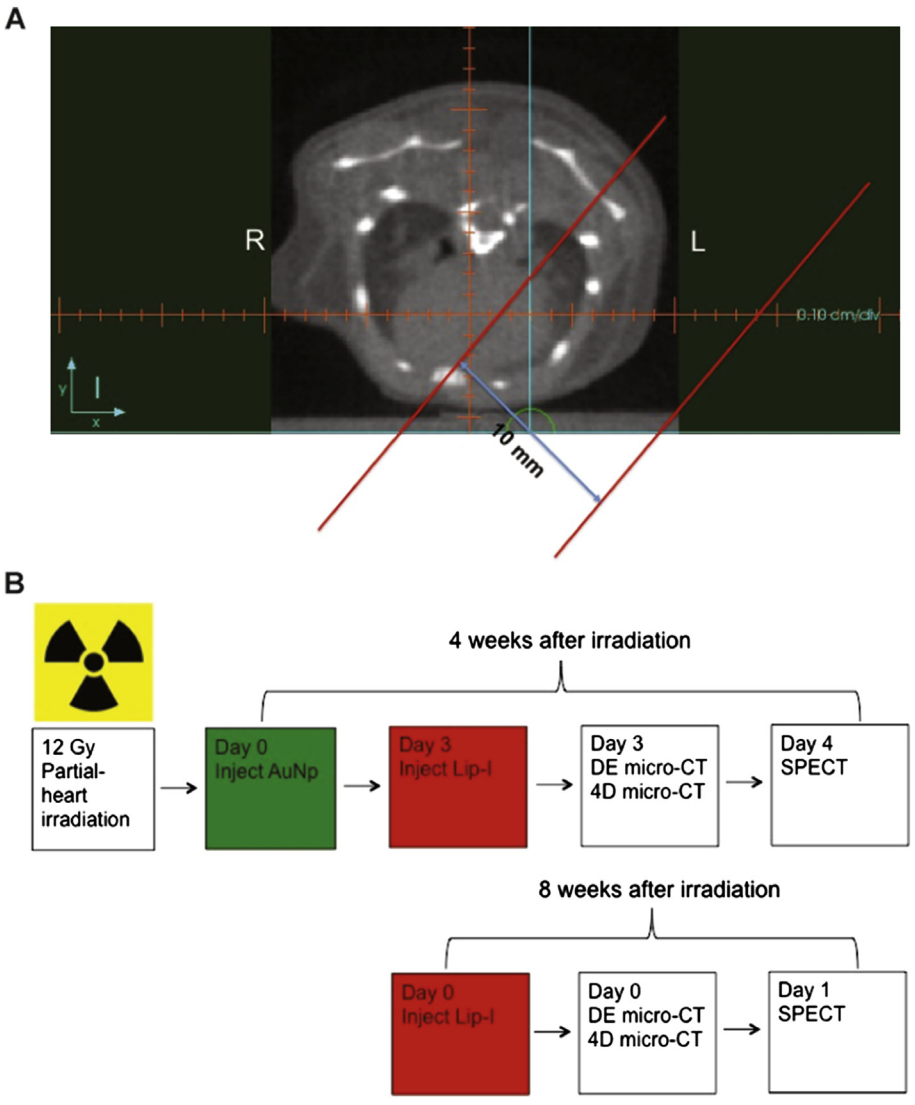

Fig. 1. Multimodality imaging of the mouse heart after partial heart irradiation. (A) Representative axial slice of the pretreatment micro-computed tomography (CT) of a mouse heart. The isocenter is placed in a reproducible position in each mouse using the axial, coronal, and sagittal images based on bony landmarks (sternum and thoracic vertebral bodies) and the heart. Then a 10-mm-wide rectangular collimator is used to deliver RT with a left posterior oblique (gantry angle = 45°) and a right anterior oblique (gantry angle = 225°) field. The tangent radiation fields are shown within the parallel red lines. (B) Schematic of the protocol for dual energy (DE)-microCT, 4-dimensional (4D)-microCT, and micro-single photon emission CT (SPECT) imaging. Four weeks after irradiation, mice were administered the gold nanoparticles (AuNp), and 3 days later the liposomal iodine (Lip-I) contrast agent. The mice were then imaged with DE-microCT and 4D-microCT. One day after CT imaging, the mice were injected with 99mTc-tetrofosmin and imaged by microSPECT. Eight weeks after irradiation, mice were administered another bolus of Lip-I and 99mTc-tetrofosmin before microCT and microSPECT imaging, respectively.

ImageJ (http://rsbweb.nih.gov/ij/). The fraction of damaged LV was computed as the ratio between the volume of damaged LV and the total volume of the myocardium in the LV.

Comprehensive methods for DE-microCT imaging and dual energy decomposition are described in Supplementary Materials (available at www.redjournal.org).

4D-microCT

Measurements of global LV function for 4D-microCT were performed with a commercially available software package that semiautomatically segments the LV over 10 phases of the cardiac cycle and provides volumetric measurements at each phase (Vitrea , version 5.2 LV Functional Analysis, Vital Images Inc., Minnetonka, MN). The LV end-diastolic (EDV) and end-systolic (ESV) volumes were converted to absolute volumes by multiplying with voxel volumes and then used to compute stroke volume (SV), ejection fraction (EF), and cardiac output (CO), as in:

$$SV = EDV - ESV;$$

$$EF = SV/EDV; \text{ and}$$

$$CO = SV \times \text{heart rate}$$

Comprehensive methods for 4D-microCT imaging are described in Supplementary Materials (available online at www.redjournal.org).

MicroSPECT

MicroSPECT acquisitions were performed with a U-SPECTII/CT system fitted with a 0.35-mm multipinhole collimator (MILabs, Utrecht, The Netherlands). The fraction of the damaged LV was computed on microSPECT by the same method as for DE-microCT.

Comprehensive methods for microSPECT imaging are described in Supplementary Materials (available online at www.redjournal.org).

Histologic analyses

Methods for sample preparation, hematoxylin and eosin staining, Masson's trichrome staining, and quantification of the average cardiomyocyte cross-sectional area have been described previously (16).

Statistics

The results are presented as mean ± SEM. Student *t* test and the Mann-Whitney test (2-tailed) were performed to compare the means and medians of 2 groups, respectively. The *R* squared values were calculated by Pearson *r* correlation. Significance was assumed at $P<.05$ and calculated with GraphPad Prism 5 (GraphPad Software, Inc).

Results

Assessing vascular permeability in the left ventricle by dual energy microCT

The DE-microCT images and their decompositions are shown in Figure 2A. Four and 8 weeks after irradiation, accumulation of AuNp was detected in the portion of the LV that was within the radiation field in Tie2Cre; $p53^{FL/-}$ mice (Fig. 2A). The fraction of damaged LV (Fig. 2B) and the mean mass of accumulated AuNp in the LV (Fig. 2C) were significantly increased in Tie2Cre; $p53^{FL/-}$ mice compared with Tie2Cre; $p53^{FL/+}$ mice 8 weeks after irradiation. In addition, in 4 of 5 Tie2Cre; $p53^{FL/-}$ mice, a time-dependent increase in the mean mass of AuNp in the LV was observed (Fig. 2D). Collectively, these results suggest that the AuNp contrast agent and delayed DE-microCT can be used to noninvasively assess the change in permeability of myocardial vessels after partial heart irradiation.

Alterations in tissue architecture of the left ventricle after partial heart irradiation

We examined the histology of the heart in Tie2Cre; $p53^{FL/+}$ and Tie2Cre; $p53^{FL/-}$ mice after the second round of imaging (approximately 10 weeks after irradiation). Masson's trichrome-stained sections showed normal tissue architecture of the myocardium and pericardium in the irradiated LV of Tie2Cre; $p53^{FL/+}$ mice (Fig. 3A and D). By contrast, in Tie2Cre; $p53^{FL/-}$ mice, although the part of the heart that was outside the field of radiation appeared normal (Fig. 3B and E), the portion within the radiation field demonstrated multifocal to extensive myocardial necrosis and fibrosis in the same mice (Fig. 3C and F). Additionally, the pericardium in the irradiated LV was thickened by collagen fibrils and infiltration of lymphocytes (Fig. 3F).

Moreover, the sections stained with hematoxylin and eosin showed that in the myocardium of Tie2Cre; $p53^{FL/+}$ mice, AuNp was exclusively within the blood vessels (Fig. 3G). By contrast, in Tie2Cre; $p53^{FL/-}$ mice, although AuNp was also exclusively within the blood vessels in the unirradiated LV fraction (Fig. 3H), extravasation of AuNp into the necrotic myocardium was observed in irradiated portions of the LV (Fig. 3I). Together, our results show that 12 Gy partial heart irradiation caused necrosis and fibrosis in the myocardium and pericardium of Tie2Cre; $p53^{FL/-}$ mice, in which extravasation of AuNp was present. These data indicate that AuNp accumulation is a specific imaging surrogate for vascular injury induced by irradiation.

Assessing myocardial perfusion by microSPECT

We also assessed myocardial perfusion in the same cohort of Tie2Cre; $p53^{FL/+}$ and Tie2Cre; $p53^{FL/-}$ mice using microSPECT. MicroSPECT imaging of Tie2Cre; $p53^{FL/-}$ mice demonstrated a decrease in myocardial perfusion in the irradiated LV, which occurred in the same region as the accumulation of AuNp (Fig. 4A). Linear regression demonstrated a significant correlation for the fraction of damaged LV measured by microSPECT and DE-microCT 8 weeks after partial heart irradiation ($R^2 = 0.97$) (Fig. 4B).

Measuring cardiac function by 4D-microCT

We also used 4D-microCT to measure several clinically important endpoints of cardiac physiology, including the LV EDV, ESV, SV, EF, and CO (22). Our results show that 4 and 8 weeks after partial heart irradiation, Tie2Cre; $p53^{FL/-}$ mice had a significant increase in both EDV and ESV and a significant decrease in EF compared with Tie2Cre; $p53^{FL/+}$ control mice (Fig. 5A and B).

At necropsy 10 weeks after irradiation, we observed a markedly increased ratio of heart weight to body weight (Fig. 5C). In addition, the average cardiomyocyte cross-sectional area in the myocardium outside the field of radiation in Tie2Cre; $p53^{FL/-}$ mice were increased compared with Tie2Cre; $p53^{FL/+}$ littermates (Fig. 5D and E). Together, the results from 4D-microCT and histology studies indicate that partial heart irradiation with 12-Gy x-rays not only caused necrosis and fibrosis within the irradiated LV of Tie2Cre; $p53^{FL/-}$ mice but also caused compensatory enlargement of surviving cardiomyocytes in the myocardium outside the field of radiation, which led to hypertrophy, dilatation, and decreased EF in the LV.

Discussion

Although the clinical manifestations of RRHD are diverse, one of the early effects of partial heart irradiation is decreased myocardial perfusion, which results from damage to the microvasculature within the irradiated heart (18). In this study, DE-microCT was used to noninvasively assess radiation-induced changes in myocardial vascular permeability by measuring the accumulation of AuNp (Fig. 2). By histology, we demonstrated

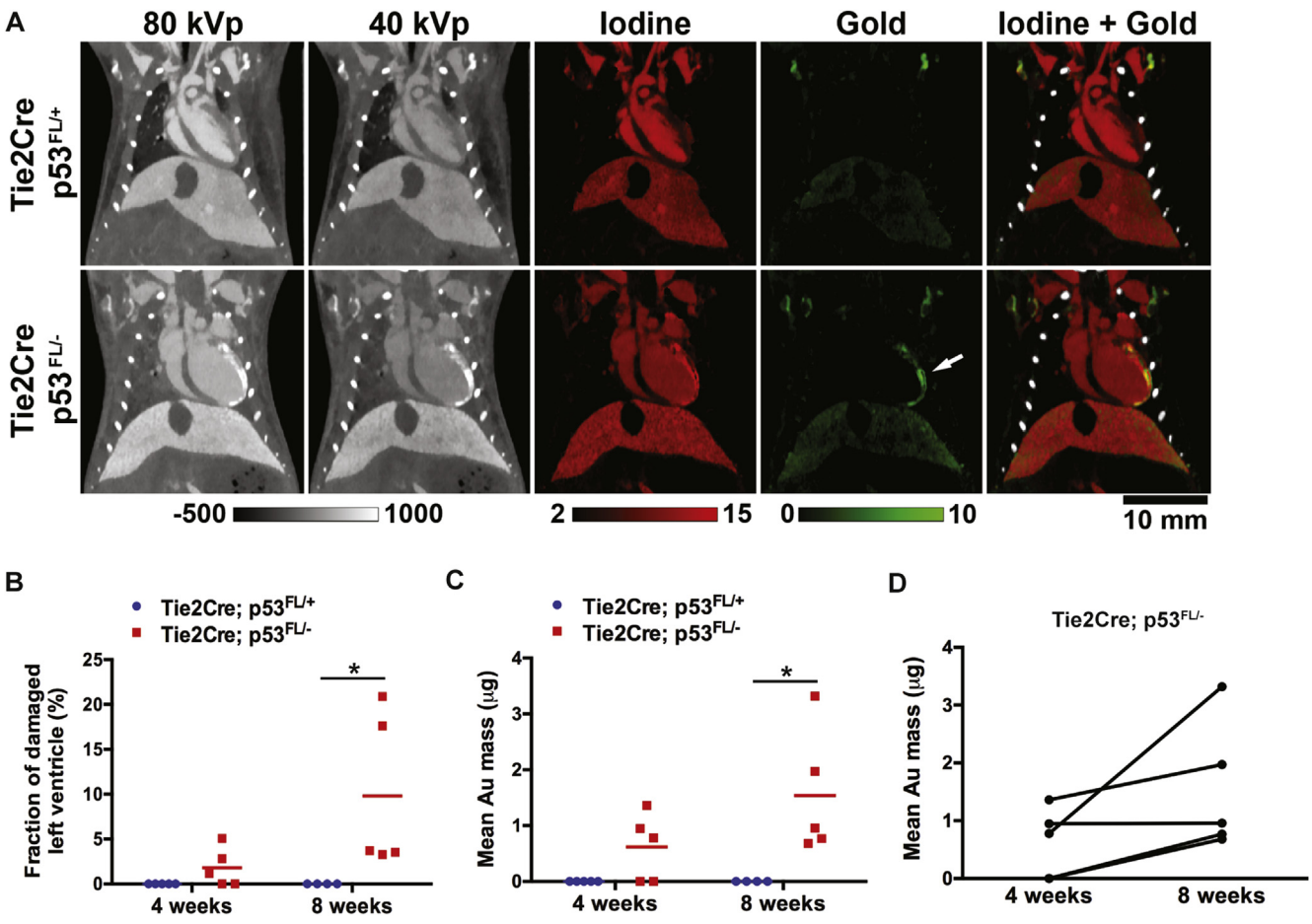

Fig. 2. Dual energy-micro-computed tomography (CT) to assess accumulation of Au nanoparticles in the left ventricle (LV). (A) Iodine maps (red) were used to contour the total volume of the LV, whereas Au maps (green) from the same animal were used to quantify the volume of the myocardium that had increased AuNp accumulation (arrow). (B) Quantification of the fraction of damaged LV and (C) of mean Au mass in the LV 4 and 8 weeks after irradiation. (D) Comparison of the mean Au mass in the LV of Tie2Cre; $p53^{FL/-}$ mice 4 and 8 weeks after irradiation. *P* values were calculated by Mann-Whitney test. $*P<.05$.

that the extravasation of AuNp occurred specifically in the irradiated myocardium and pericardium that became necrotic and fibrotic 10 weeks after irradiation (Fig. 3). Additionally, the accumulation of AuNp in the irradiated LV detected by DE-microCT significantly correlated with defects in myocardial perfusion measured by microSPECT (Fig. 4). Therefore, our results indicate that DE-microCT with AuNp can noninvasively assess radiation-induced damage to the myocardial vasculature in mice.

In the same cohort of mice, blood pool Lip-I and 4D-microCT enabled us to measure LV volumes over the cardiac cycle to assess cardiac function. Four and 8 weeks after partial heart irradiation, Tie2Cre; $p53^{FL/-}$ mice showed a significant decrease in EF compared with Tie2Cre; $p53^{FL/+}$ littermates (Fig. 5A and B). The decrease in EF was associated with LV dilation and hypertrophy. Nevertheless, in Tie2Cre; $p53^{FL/-}$ mice there was no significant decrease in SV and CO, likely as a result of compensatory changes in the heart as reflected by the increase in both EDV and ESV and the length of follow-up.

In our prior studies we showed that after whole heart irradiation, multifocal myocardial necrosis and systolic dysfunction developed in Tie2Cre; $p53^{FL/-}$ mice (16). However, the LVs in those mice were not dilated and showed only limited fibrosis in the myocardium and pericardium. By contrast, in this study we found that after partial heart irradiation, LV dilation developed in Tie2Cre; $p53^{FL/-}$ mice (Fig. 5A and B), as did extensive fibrosis in the irradiated myocardium and pericardium (Fig. 3C and F), which suggest more of a chronic injury. Together, these results suggest that compared with whole heart irradiation, partial heart irradiation may cause different changes in cardiac physiology and pathology, which better model pericarditis and myocardial injury that can occur in patients receiving left chest wall irradiation with tangent fields.

In this study, we performed partial heart irradiation with 12-Gy x-rays to model radiation-induced myocardial injury in Tie2Cre; $p53^{FL/-}$ mice, in which endothelial cells are sensitive to radiation. The histologic manifestations of cardiac injury in this model, which include myocardial fibrosis and pericarditis, mimic the pathologic changes observed in humans (18) and wild-type mice (15) after heart irradiation. However, in wild-type animals exposed to whole heart irradiation, cardiac injury varies with the total dose and time after irradiation (7, 13, 15, 23). Therefore, in future studies we will use the imaging techniques developed in this study to characterize the physiologic and cellular events that lead to cardiac injury in wild-type mice after partial heart irradiation with a more clinically relevant radiation dose, such as 2 Gy/day up to 50 Gy.

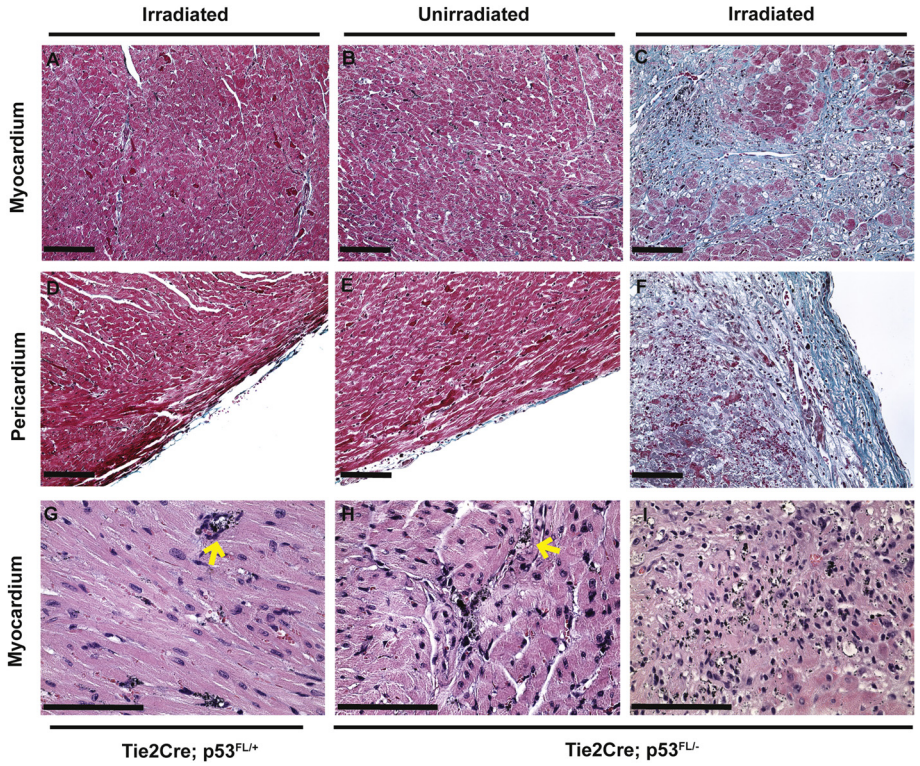

Fig. 3. Histologic examination of the myocardium and pericardium 10 weeks after partial heart irradiation. Masson's trichrome staining demonstrated relatively normal-appearing myocardium and pericardium (red) in the left ventricle (LV) of Tie2Cre; $p53^{FL/+}$ mice that were irradiated (A and D) and of Tie2Cre; $p53^{FL/-}$ mice outside the field of irradiation (B and E). By contrast, in irradiated LV of Tie2Cre; $p53^{FL/-}$ mice, collagen fibers (blue) were present in the myocardium (C) and pericardium (F). Hematoxylin and eosin staining demonstrated that gold nanoparticles (AuNp) (small black particles) were restricted within blood vessels (yellow arrow) in the LV of Tie2Cre; $p53^{FL/+}$ mice that were irradiated (G) and of Tie2Cre; $p53^{FL/-}$ mice that outside the field of irradiation (H). Of note, in the irradiated LV of Tie2Cre; $p53^{FL/-}$ mice, extravasation of AuNp was observed in necrotic and fibrotic areas in the myocardium (I). Scale bar, 100 μm.

It is possible that the phenotype we observed in this study was influenced by the additional radiation exposure from microCT and microSPECT (approximately 2.18 Gy per mouse for the entire study). This additional radiation exposure represents 18% of the partial heart irradiation dose. This dose was not sufficient to elicit radiation injury to the part of the heart in Tie2Cre; $p53^{FL/-}$ mice outside the tangent fields (Fig. 3), but it may have additive effects on the myocardium within the tangent fields. Therefore, it will be important to limit the number of scans or to choose either microCT or microSPECT in future studies to minimize the radiation exposure from imaging.

In conclusion, our results show that DE-microCT and 4D-microCT with nanoparticle-based contrast agents are promising approaches for the assessment of changes in vascular permeability and cardiac function in the preclinical setting. These imaging approaches may be useful in identifying patients treated with RT who have experienced vascular injury in the heart that may lead to radiation-related heart disease.

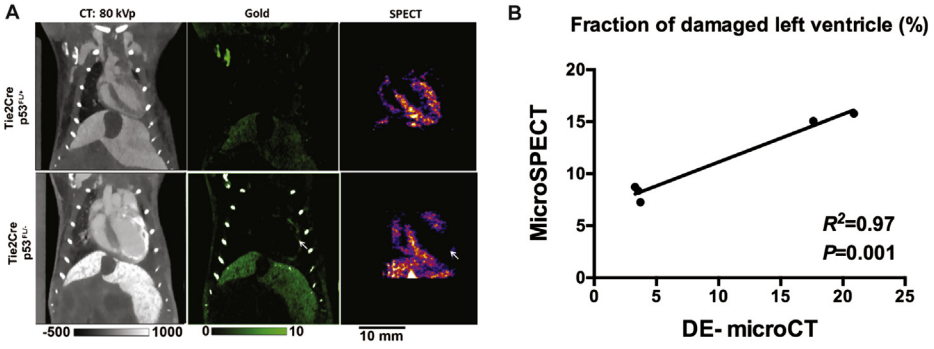

Fig. 4. Micro-single photon emission computed tomography (SPECT) scans to assess changes in myocardial perfusion. (A) Representative dual energy (DE)-microCT (green) and SPECT images of the heart 8 weeks after 12 Gy partial heart irradiation. Note that the area of decreased perfusion on SPECT (white arrow) matches the region of AuNp accumulation on DE-microCT. (B) Correlation analysis of the fraction of damaged LV that was assessed by SPECT and DE microCT. *R* squared and *P* values were calculated with Pearson *r* correlation.

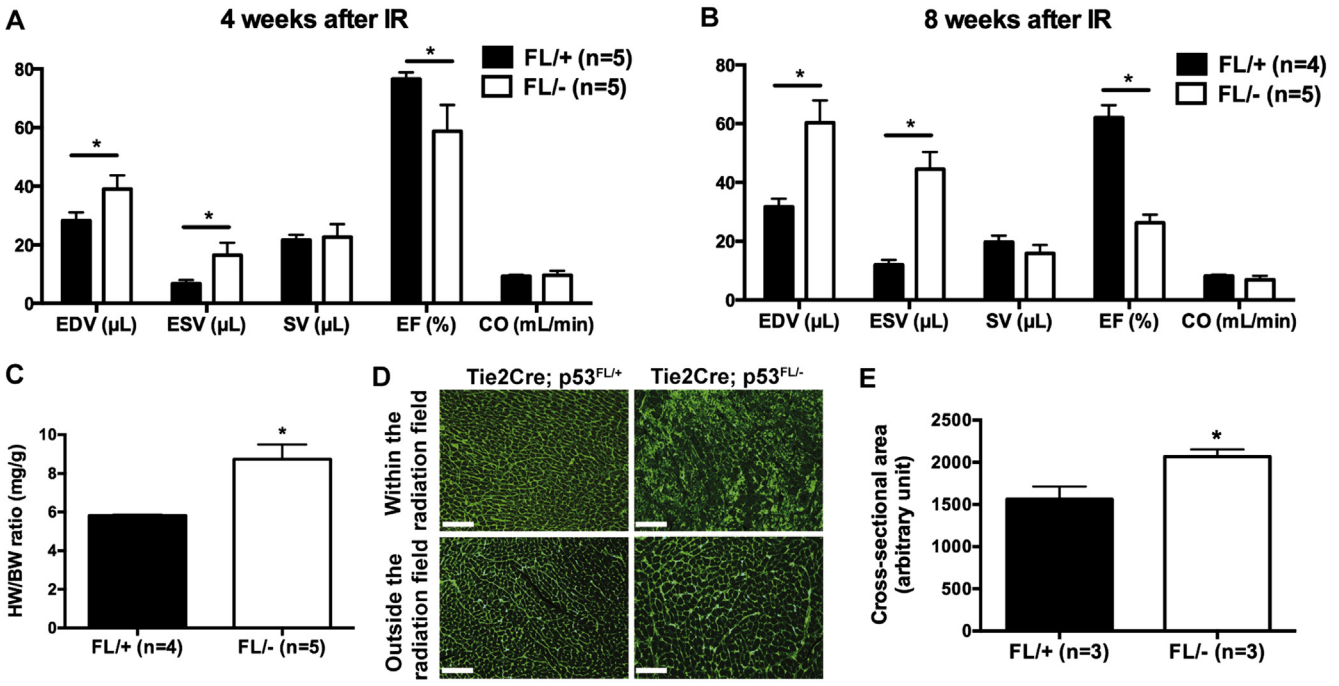

Fig. 5. Four-dimensional (4D)-micro-computed tomography (CT) scans to examine changes in cardiac function after partial heart irradiation (IR). (A and B) 4D-micoCT was performed 4 and 8 weeks after irradiation to assess end-diastolic volume (EDV), end-systolic volume (ESV), stroke volume (SV), ejection fraction (EF), and cardiac output (CO) of the left ventricle (LV). (C) Ratio of heart weight to body weight (HW/BW) of Tie2Cre; $p53^{FL/+}$ and Tie2Cre; $p53^{FL/-}$ mice 10 weeks after irradiation. (D) Representative images of wheat germ agglutinin (WGA)-stained myocardium that was within or outside of the radiation field. Scale bar, 100 μm. (E) Quantification of cardiomyocyte cross-sectional area in WGA-stained myocardium that was outside of the radiation field. Data are presented as mean ± SEM (n = 3 mice per group). *$P < .05$ by Student t test.

References

1. Favourable and unfavourable effects on long-term survival of radiotherapy for early breast cancer: An overview of the randomised trials. Early Breast Cancer Trialists' Collaborative Group. *Lancet* 2000;355:1757-1770.
2. Fisher B, Anderson S, Bryant J, et al. Twenty-year follow-up of a randomized trial comparing total mastectomy, lumpectomy, and lumpectomy plus irradiation for the treatment of invasive breast cancer. *N Engl J Med* 2002;347:1233-1241.
3. Darby SC, McGale P, Taylor CW, et al. Long-term mortality from heart disease and lung cancer after radiotherapy for early breast cancer: Prospective cohort study of about 300,000 women in US SEER cancer registries. *Lancet Oncol* 2005;6:557-565.
4. Cuzick J, Stewart H, Rutqvist L, et al. Cause-specific mortality in long-term survivors of breast cancer who participated in trials of radiotherapy. *J Clin Oncol* 1994;12:447-453.
5. EBCTCG. Effects of radiotherapy and surgery in early breast cancer: An overview of the randomized trials. *New Engl J Med* 1995;333:1444-1455.
6. Darby SC, Ewertz M, McGale P, et al. Risk of ischemic heart disease in women after radiotherapy for breast cancer. *N Engl J Med* 2013;368:987-998.
7. Schultz-Hector S, Trott KR. Radiation-induced cardiovascular diseases: Is the epidemiologic evidence compatible with the radiobiologic data? *Int J Radiat Oncol Biol Phys* 2007;67:10-18.
8. Seddon B, Cook A, Gothard L, et al. Detection of defects in myocardial perfusion imaging in patients with early breast cancer treated with radiotherapy. *Radiother Oncol* ;64; 2002:53-63.
9. Marks LB, Yu X, Prosnitz RG, et al. The incidence and functional consequences of RT-associated cardiac perfusion defects. *Int J Radiat Oncol Biol Phys* 2005;63:214-223.
10. Prosnitz RG, Hubbs JL, Evans ES, et al. Prospective assessment of radiotherapy-associated cardiac toxicity in breast cancer patients: Analysis of data 3 to 6 years after treatment. *Cancer* 2007;110:1840-1850.
11. Fajardo LF, Stewart JR. Pathogenesis of radiation-induced myocardial fibrosis. *Lab Invest* 1973;29:244-257.
12. Fajardo LF, Stewart JR. Experimental radiation-induced heart disease. I. Light microscopic studies. *Am J Pathol* 1970;59:299-316.
13. Lauk S, Kiszel Z, Buschmann J, et al. Radiation-induced heart disease in rats. *Int J Radiat Oncol Biol Phys* 1985;11:801-808.
14. Yeung TK, Lauk S, Simmonds RH, et al. Morphological and functional changes in the rat heart after X irradiation: Strain differences. *Radiat Res* 1989;119:489-499.
15. Seemann I, Gabriels K, Visser NL, et al. Irradiation induced modest changes in murine cardiac function despite progressive structural damage to the myocardium and microvasculature. *Radiother Oncol* 2012;103:143-150.
16. Lee CL, Moding EJ, Cuneo KC, et al. p53 functions in endothelial cells to prevent radiation-induced myocardial injury in mice. *Sci Signal* 2012;5. ra52.
17. Kirsch DG, Santiago PM, di Tomaso E, Sullivan JM, Hou WS, Dayton T, Jeffords LB, Sodha P, Mercer KL, Cohen R, Takeuchi O, Korsmeyer SJ, Bronson RT, Kim CF, Haigis KM, Jain RK, Jacks T. p53 controls radiation-induced gastrointestinal syndrome in mice independent of apoptosis. *Science* 2010 Jan 29;327(5965):593-59610. 1126/science.1166202.
18. Stewart FA, Hoving S, Russell NS. Vascular damage as an underlying mechanism of cardiac and cerebral toxicity in irradiated cancer patients. *Radiat Res* 2010;174:865-869.

19. Darby SC, Cutter DJ, Boerma M, et al. Radiation-related heart disease: Current knowledge and future prospects. *Int J Radiat Oncol Biol Phys* 2010;76:656-665.
20. Moding EJ, Clark DP, Qi Y, et al. Dual-energy micro-computed tomography imaging of radiation-induced vascular changes in primary mouse sarcomas. *Int J Radiat Oncol Biol Phys* 2013;85:1353-1359.
21. Mukundan S Jr, Ghaghada KB, Badea CT, et al. A liposomal nanoscale contrast agent for preclinical CT in mice. *AJR Am J Roentgenol* 2006;186:300-307.
22. Libutti SK, Paciotti GF, Byrnes AA, et al. Phase I and pharmacokinetic studies of CYT-6091, a novel PEGylated colloidal gold-rhTNF nanomedicine. *Clin Cancer Res* 2010;16:6139-6149.
23. Busch S, Johnson TR, Wintersperger BJ, et al. Quantitative assessment of left ventricular function with dual-source CT in comparison to cardiac magnetic resonance imaging: Initial findings. *European Radiology* 2008;18:570-575.
24. Yeung TK, Hopewell JW. Effects of single doses of radiation on cardiac function in the rat. *Radiother Oncol* 1985;3:339-345.